Two-dimensional argon metastable density measurements in a radio frequency plasma reactor by planar laser-induced fluorescence imaging

Brian K. McMillin[a] and Michael R. Zachariah
Chemical Science and Technology Laboratory, National Institute of Standards and Technology, Gaithersburg, Maryland 20899

(Received 8 December 1994; accepted for publication 20 February 1995)

Two-dimensional, relative measurements of the argon $1s_5$ metastable density distribution were obtained in a low-pressure, 13.56 MHz, parallel-plate, Gaseous Electronics Conference reference cell discharge using planar laser-induced fluorescence imaging. For the conditions examined (pure argon, 75–300 V, 13.3–133.3 Pa), the measured density fields show significant radial and axial variations that depend more strongly on pressure than applied voltage. Generally speaking, the metastable density increases radially from the center to the edge of the discharge by ~10%–30%. As the pressure is increased, the peak metastable density increases by ~4 times and the axial distribution changes from a center-peaked parabolic-like profile to an asymmetric profile peaked near the powered electrode. Comparisons of centerline metastable and excited-state emission profiles indicate that, while the metastable distribution is largely determined by the spatially dependent electron-impact excitation function, variations in quenching can significantly affect the resulting metastable density profile at some conditions. © *1995 American Institute of Physics.*

INTRODUCTION

Low-pressure, radio-frequency (rf) plasmas are used extensively for etching and deposition of thin films during microelectronics fabrication. As a result, a great deal of experimental[1] and numerical modeling[1–5] research in recent years has been directed at developing a better understanding of the chemistry and physics in these plasmas. The majority of gas-phase species concentration measurements in these plasmas, however, have been limited to optical emission, line-of-sight absorption, or single-point laser-induced fluorescence.[1,6] To our knowledge, the only complete two-dimensional (2D) species measurements in an rf plasma are the absorption-based helium metastable density measurements reported by Greenberg and Hebner.[7] As modeling work progresses toward multidimensional simulations, a more extensive (i.e., 2D) experimental data base will be necessary for verification of these models.

The purpose of this study was to use planar laser-induced fluorescence (PLIF) imaging to map the spatially resolved, 2D argon metastable density field in a low-pressure rf glow discharge. Only a few previous experimental studies[8–12] have examined the argon metastable density in rf plasmas, and those have been limited to one-dimensional spatial profiles and/or measurements at the plasma center. The present time-averaged, relative measurements are of interest as they provide additional insight into the plasma uniformity, through 2D visualization of the metastable density distribution. In addition, the measurements cover a wide range of conditions and were performed in a well-characterized reactor (the Gaseous Electronics Conference or GEC rf reference cell[13]), which should make them useful as a data source for validation of plasma models.

In this study we focused on pure argon plasmas since they are relatively simple, extensively studied, and reasonably amenable to modeling. The metastables are generally important in plasmas containing rare gases, because, with their relatively long radiative lifetime and high (electronic) potential energy, they can transfer a considerable amount of energy through gas phase collisions. For argon, two of the electronically excited states are metastable (the $1s_3$ and $1s_5$ states within the $4s$ level; see Fig. 1); that is, for these states, no electric dipole optical transitions to the ground state are allowed. With radiative decay forbidden, these excited states are long-lived (milliseconds) at typical operating conditions within a glow discharge. As a result, in argon plasmas the metastables provide electrons (and ions) through step-wise ionization and metastable pooling processes which help sustain the discharge.[3] In addition, in argon/molecular discharge mixtures, collisions with metastables can lead to Penning ionization, dissociation, and/or excitation of the molecular species.[14]

In the following, we first describe the experimental setup and then discuss the results of the metastable density measurements; for more details on the measurement technique, the reader is referred to Refs. 1 and 6 regarding laser-induced fluorescence in glow discharges, and Ref. 15 regarding PLIF imaging in general. In addition, line-of-sight-integrated, centerline (axial) emission profiles of excited-state argon are also presented and used to help interpret the metastable measurements. The results presented here encompass a pressure range of 13.3–133.3 Pa and applied peak-to-peak voltages of 75–300 V.

EXPERIMENTAL DETAILS

The experiments were conducted using a GEC rf reference cell, which has been described in detail elsewhere.[13] Briefly, the GEC cell is an asymmetrically driven, parallel-plate system using 10.2-cm-diameter aluminum electrodes

[a]National Research Council NIST postdoctoral research associate, 1993–present.

 0021-8979/95/77(11)/5538/7/$6.00

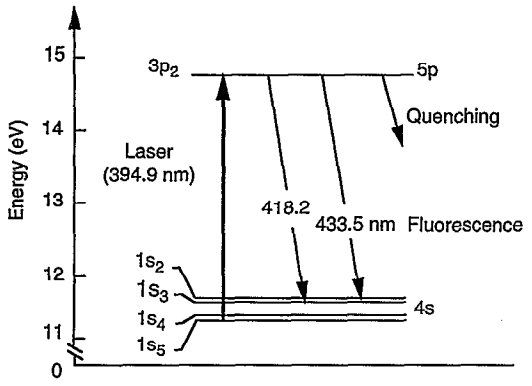

FIG. 1. Partial energy level diagram of neutral argon depicting the ground, $4s$, and $5p$ states, labelled in Paschen notation. The laser excitation and fluorescence transitions used in these experiments are indicated by arrows in the diagram.

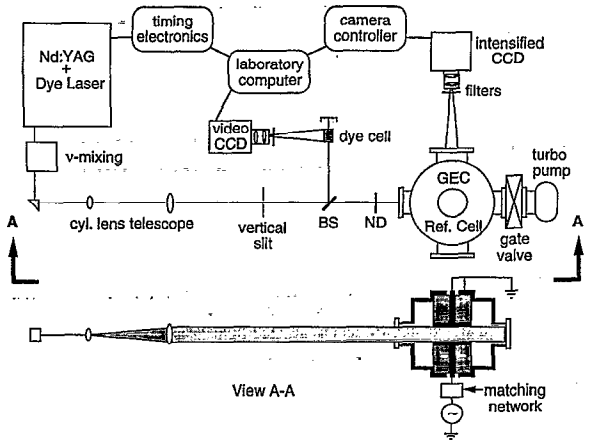

FIG. 2. Schematic diagram of the experimental setup.

with a nominal 2.54 cm interelectrode spacing. A turbomolecular pump evacuates the chamber to a base pressure of $\sim 1\times10^{-5}$ Pa (8×10^{-8} Torr) prior to experiments, and a mechanical vacuum pump maintains the (13.3–133.3 Pa) pressure during experiments. The feed gas is introduced through a showerhead arrangement of holes in the upper electrode. The lower electrode is powered by a 13.56 MHz rf power supply coupled through a matching network and an isolating rf filter. The upper electrode and the remainder of the chamber is grounded.

Voltage and current waveforms were measured at the base of the powered electrode and recorded with a digital oscilloscope. Using an equivalent circuit model of the GEC cell[16] and the accompanying external circuitry, these waveforms were Fourier analyzed to determine the magnitudes and relative phases of the voltage and current at the surface of the powered electrode. Table I summarizes the electrical measurements for the plasma conditions examined here. Included in the table are the amplitudes of the fundamental Fourier components of the voltage and current waveforms, their relative phases, and the magnitudes of the dc self-bias potential and power dissipated in the plasma.

TABLE I. Amplitudes (half of peak-to-peak) of the fundamental components of the voltage (V_1) and current (I_1) waveforms at the surface of the powered electrode, the phase (ϕ_1) of the voltage with respect to current, the dc self-bias (V_{dc}), and the power (P) dissipated in the plasma as a function of gas pressure and the applied peak-to-peak rf voltage (V_{rf}).

Pressure (Pa)	V_{rf} (V)	V_1 (V)	I_1 (mA)	ϕ_1 (deg)	V_{dc} (V)	P (W)
13.3	75	40.5	80	−70.9	−15.6	0.5
	150	82.9	168	−77.9	−54.6	1.5
	200	110.7	209	−79.4	−80.5	2.1
	300	167.0	292	−81.1	−133.6	3.8
33.3	200	112.7	337	−78.3	−79.6	3.4
66.7	200	113.6	491	−78.1	−75.0	5.7
133.3	75	41.4	145	−66.7	−6.9	1.2
	150	84.9	462	−73.7	−42.6	5.5
	200	114.3	680	−75.4	−69.4	9.8
	300	173.5	1050	−76.6	124.1	21.1

The metastable density fields were determined using PLIF imaging, a technique which provides an efficient means of simultaneously measuring a given species concentration over a large area within the discharge, with excellent spatial resolution. As shown schematically in Fig. 2, the laser excitation source was a Nd:YAG pumped dye laser. The dye laser output was frequency mixed with the residual 1.06 μm beam from the pump laser, using a KD*P crystal, to produce pulses at ~395 nm (10 ns, 3 mJ, ~1 cm^{-1}). The output beam was then expanded vertically using a cylindrical telescope and apertured with a slit to yield a 2×25 mm sheet, with nearly uniform spatial energy distribution. The laser sheet was also attenuated using neutral density filters so that the fluence entering the GEC cell was less than ~0.1 mJ/cm^2. This relatively low laser fluence combined with the uniform energy distribution in the sheet was used to reduce measurement uncertainties due to fluorescence saturation. The laser energy was monitored during the experiments by directing a 5% reflection of the laser sheet onto a static dye cell, and recording the resulting fluorescence with a video CCD camera and framegrabber computer board.

The argon $1s_5$ metastable level density was measured by exciting the $1s_5 \rightarrow 3p_2$ transition at ~394.9 nm and detecting the fluorescence at ~418 and ~433 nm (see Fig. 1). The fluorescence was collected at a right angle to the illumination plane and imaged onto an intensified, cooled CCD camera (576×384 pixels, each 23 μm square) using an f/4.5 lens. A 410 nm long-pass filter was used to reject the laser scattering and a 450 nm short-pass filter was used to reduce the plasma emission reaching the camera. The intensifier gate was set to ~500 ns to temporally integrate the entire fluorescence decay. The PLIF images obtained were 1000 laser shot averages and were spatially averaged 2×2 pixels, leading to a nominal axial and radial resolution of ~200 μm.

During data reduction of the raw fluorescence images, the plasma emission and camera dark background were first subtracted, and then the background-corrected images were normalized for the detector spectral response and flatfield uniformity, laser energy distribution, and fluorescence yield. The spectral response/flatfield correction was obtained by imaging uniform light from a standard, diffuse tungsten lamp

through the filters noted above. The laser energy distribution corrections were applied by re-mapping images of the static dye cell from the video CCD to the intensified CCD coordinates, based on calibration images obtained with the laser sheet masked. To determine the corrections for excited-state quenching, the fluorescence yields were measured at each condition by monitoring the fluorescence decay from the center of the discharge using a photomultiplier and digital oscilloscope. These corrections for the fluorescence yield were necessary because the relatively long radiative lifetime of the $5p$ $(3p_2)$ state (154 ns)[17] results in significant collisional quenching of the excited-state fluorescence.

In correcting the metastable images for excited-state quenching, we assumed that the fluorescence yield was not a function of position within the discharge. This is a reasonable assumption here because a comparison of collisional quenching rates indicates that the ground state argon dominates the fluorescence quenching. More specifically, we estimate that the fluorescence quenching rate coefficient by argon $(Q_{Ar}=N_{Ar}k_{Ar})$ ranges from 10^6–10^7 s^{-1} over the pressure range considered here, based on a measured argon quenching rate constant, k_{Ar}, of $\sim 6\times10^{-10}$ cm^3/s that was found to be independent of applied voltage, and an estimated argon density, N_{Ar}, of 10^{15}–10^{16} cm^{-3}, assuming a gas temperature of 350 K. In contrast, we estimate that the fluorescence quenching rate coefficient by electrons $(Q_e=N_ek_e)$ is $\sim 10^3$ s^{-1}, assuming an electron number density, N_e, of $\sim 10^{10}$ cm^{-3} and an electron quenching rate constant[18] (k_e) of 2×10^{-7} cm^3/s.

Thus, because neutral argon dominates the fluorescence quenching, and its concentration and temperature are expected to be essentially uniform, the fluorescence yield is not expected to vary within the discharge. For completeness, we note that our measured value for argon $5p$ quenching is comparable to, although 2–3 times larger than, the value previously reported by Inoue *et al.*[19]

RESULTS AND DISCUSSION

Relative, 2D measurements of the argon $1s_5$ metastable density were obtained in experiments with a 10 sccm argon (99.999% purity) flowrate, pressures of 13.3, 33.3, 66.7, and 133.3 Pa (100, 250, 500, and 1000 mTorr), and nominal applied peak-to-peak voltages of 75, 100, 150, 200, and 300 V. The estimated uncertainty in the relative number densities reported here is ~10% based on the reproducibility of the measurements. The absolute metastable density was not determined in these experiments, although previous laser absorption measurements[9] at similar conditions have indicated that the argon $1s_5$ metastable density is on the order of 10^{11} cm^{-3}.

Figure 3 shows contour plots of the argon $1s_5$ metastable density distribution measured as a function of pressure at a nominal 200 V applied rf voltage. In the figure the $z=0$ and $z=2.25$ cm axial locations correspond to the powered and grounded electrodes, respectively. As shown in the figure, the metastable density varies considerably both with radial and axial position within the discharge. Over this pressure range, the metastable density increases radially by ~10%–30% from the center toward the outer edge of the plasma. In addition, the peak concentration shifts slightly outward and closer to the radial edge of the electrode as the pressure is increased. The higher metastable density near the edge of the powered electrode presumably results from the enhanced electric field there,[20] which produces more energetic electrons and, thus, more metastables through electron-impact collisions.

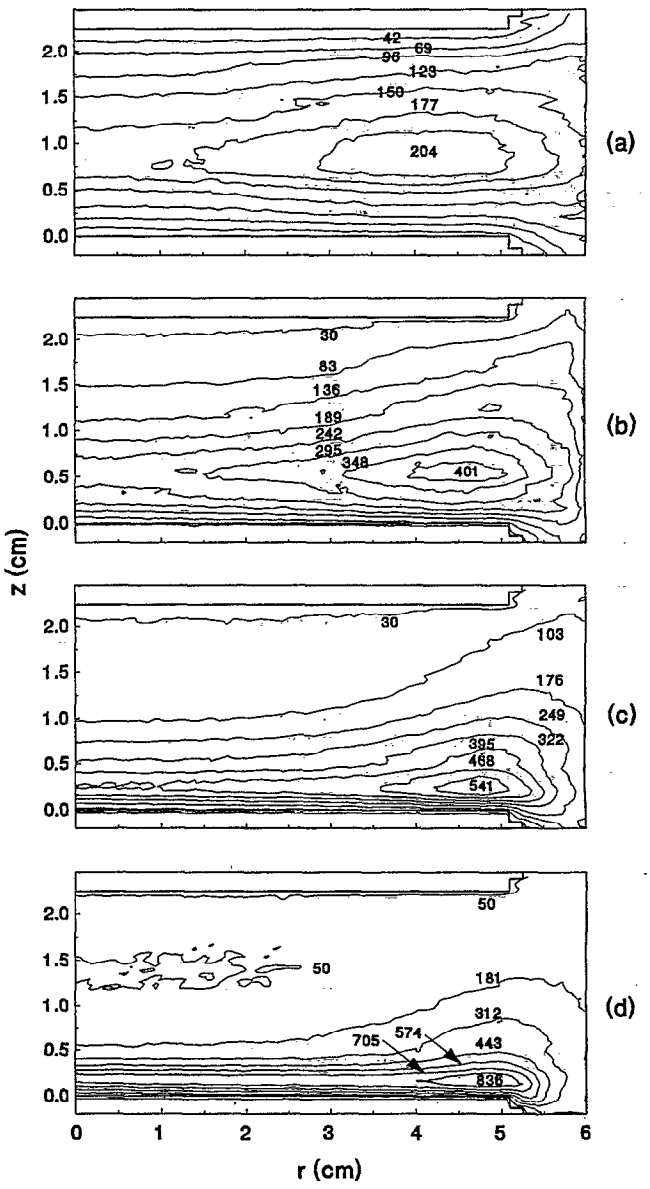

FIG. 3. Contour plots of the argon $1s_5$ metastable relative density distributions in the GEC cell with an applied rf voltage of 200 V and pressures of (a) 13.3 Pa (100 mTorr), (b) 33.3 Pa (250 mTorr), (c) 66.7 Pa (500 mTorr), and (d) 133.3 Pa (1000 mTorr).

These contour plots also show that the axial distribution changes significantly as a function of pressure as well. At 13.3 Pa, for example, the metastable density profile is nearly symmetric with the peak near the center of the discharge, but as the pressure is increased the profile becomes more asymmetric, with the peak approaching the powered electrode. This trend in the metastable distribution is illustrated more clearly by the centerline profiles shown in Fig. 4. In these

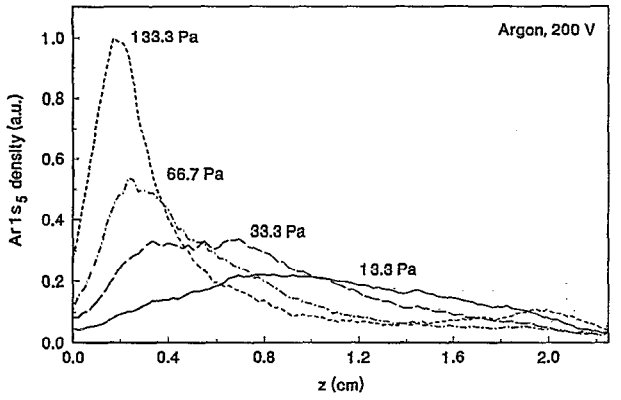

FIG. 4. Axial centerline profiles of the argon $1s_5$ metastable relative density distributions as a function of pressure at an applied rf voltage of 200 V (taken from Fig. 3).

profiles, we observe that the peak metastable density increases by a factor of ~4, while the metastable density at the plasma center decreases by a factor of ~2, as the pressure is increased from 13.3 to 133.3 Pa.

Figures 5 and 6 show 2D contour plots of the argon $1s_5$ metastable density fields as a function of applied rf voltage at two pressures, 13.3 and 133.3 Pa. As illustrated in these figures, changes in the applied voltage are found to have a less significant effect on the metastable distribution than changes in pressure. Typically, as the voltage is increased the peak metastable density increases; the metastable density distribution becomes more uniform radially, and the axial distribution tends to shift slightly toward the powered electrode. This shift in the axial distribution is seen more clearly in Fig. 7, which shows the centerline metastable density profiles for 13.3 and 133.3 Pa.

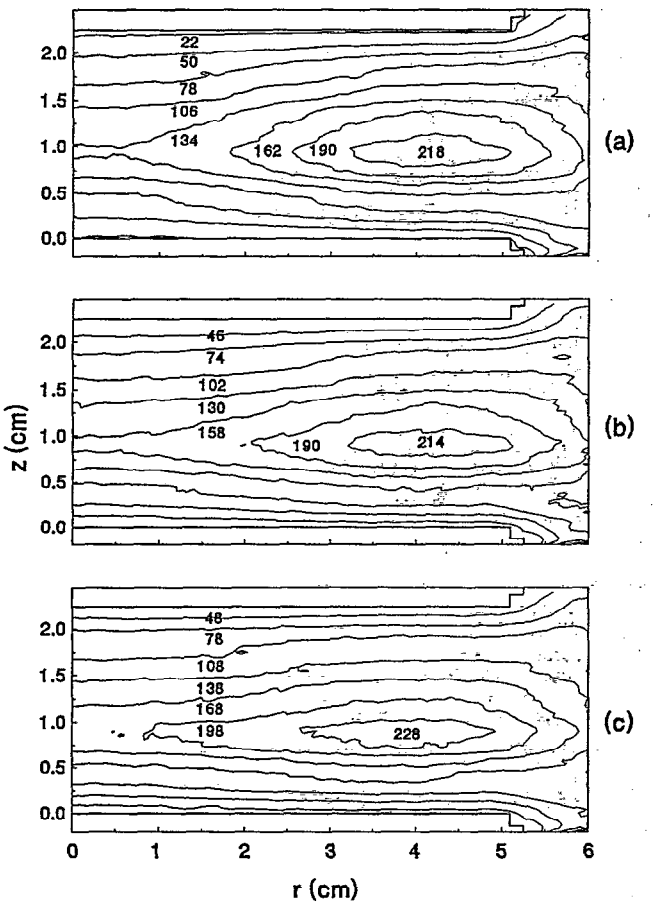

FIG. 5. Contour plots of the argon $1s_5$ metastable relative density distributions in the GEC cell at a pressure of 13.3 Pa (100 mTorr) and applied rf voltages of (a) 75 (b) 150, and (c) 300 V.

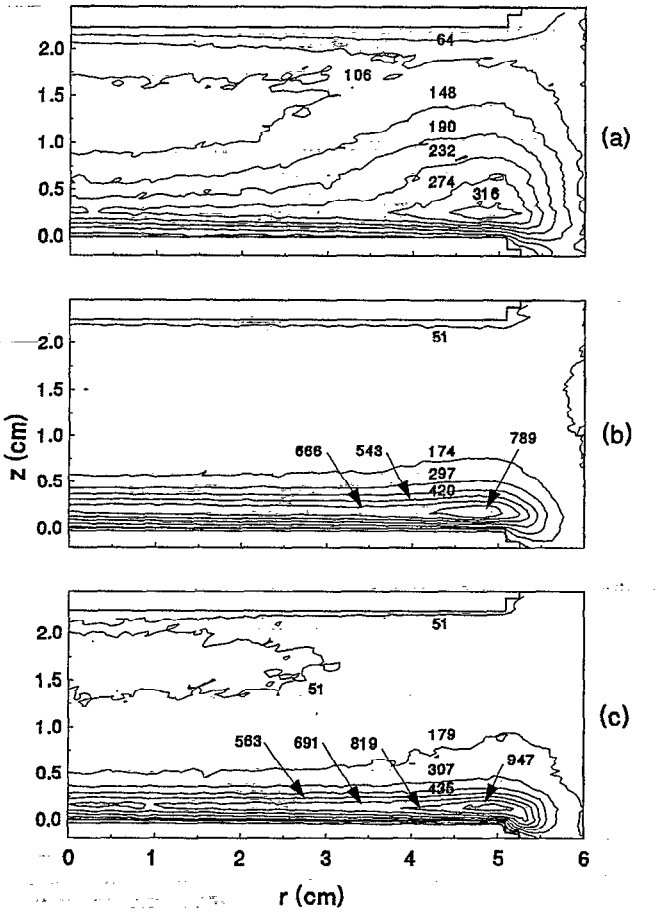

FIG. 6. Contour plots of the argon $1s_5$ metastable relative density distributions in the GEC cell at a pressure of 133.3 Pa (1000 mTorr) and applied rf voltages of (a) 75, (b) 150, and (c) 300 V.

In Fig. 7 we also observe that the peak metastable density at 13.3 Pa increases monotonically by ~30% as the applied voltage is increased from 75–300 V. Although not shown, similar and somewhat larger monotonic increases were also observed at 33.3 and 66.7 Pa as well. For the 133.3 Pa cases, however, the peak metastable density shows a nonmonotonic behavior: it increases with applied voltage over 75–200 V, and then decreases with applied voltage over 200–300 V.

In general, these observed changes in the steady-state metastable density result from a combination of changes in the spatially dependent rates of production and destruction of metastables. In argon glow discharges, the metastables are largely formed by direct electron-impact excitation, although cascading from more highly excited states can also be a significant production mechanism at some conditions.[21,22] At

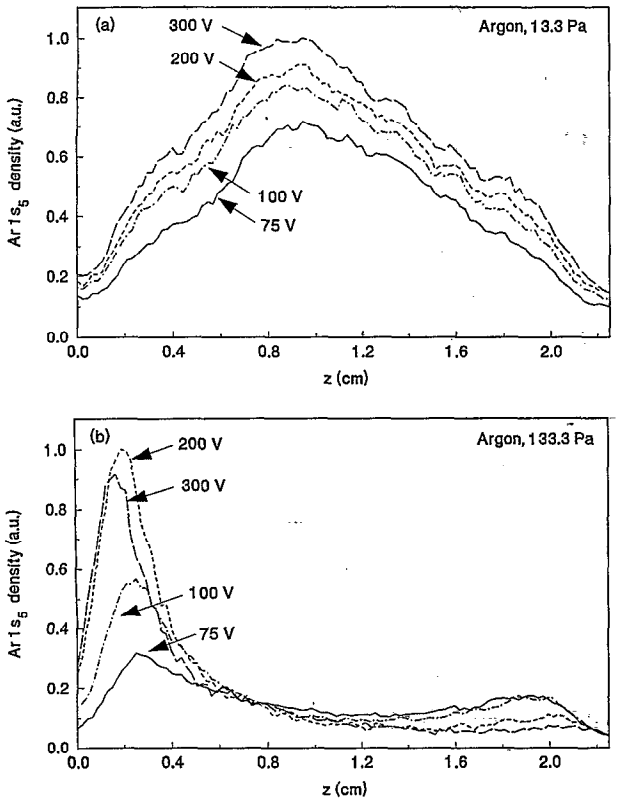

FIG. 7. Axial centerline profiles of the argon metastable relative density distributions as a function of applied rf voltage at pressures of (a) 13.3 Pa (100 mTorr) and (b) 133.3 Pa (1000 mTorr), taken from Figs. 5 and 6.

typical conditions of interest here, the primary loss mechanisms for metastables include electron quenching (to nearby resonant and higher electronic states) and diffusion to the walls.[3,10] Other loss mechanisms of lesser importance include stepwise ionization, metastable pooling, two- and three-body quenching, and superelastic electron quenching.[3] These processes are summarized as follows:

$$\mathrm{Ar}+e\rightarrow \mathrm{Ar}_m+e \quad \text{(ground state excitation)},$$

$$\mathrm{Ar}+e\rightarrow \mathrm{Ar}^*+e\rightarrow \mathrm{Ar}_m+h\nu+e \quad \text{(cascade excitation)},$$

$$\mathrm{Ar}_m+e\rightarrow \mathrm{Ar}_r+e\rightarrow \mathrm{Ar}+h\nu+e$$

(quenching to resonant; radiative decay),

$$\mathrm{Ar}_m+e\rightarrow \mathrm{Ar}^*+e\rightarrow \mathrm{Ar}_r+h\nu+e$$

(quenching to higher states; radiative decay),

$$\mathrm{Ar}_m+e\rightarrow \mathrm{Ar}^++e \quad \text{(stepwise ionization)},$$

$$\mathrm{Ar}_m+e\rightarrow \mathrm{Ar}+e \quad \text{(superelastic electron quenching)},$$

$$\mathrm{Ar}_m+\mathrm{Ar}_m\rightarrow \mathrm{Ar}^++\mathrm{Ar} \quad \text{(metastable pooling)},$$

$$\mathrm{Ar}_m+\mathrm{Ar}\rightarrow \mathrm{Ar}+\mathrm{Ar} \quad \text{(two-body quenching)},$$

$$\mathrm{Ar}_m+2\mathrm{Ar}\rightarrow \mathrm{Ar}+\mathrm{Ar}+\mathrm{Ar} \quad \text{(three-body quenching)},$$

$$\mathrm{Ar}_m+\mathrm{wall}\rightarrow \mathrm{Ar} \quad \text{(surface de-excitation)},$$

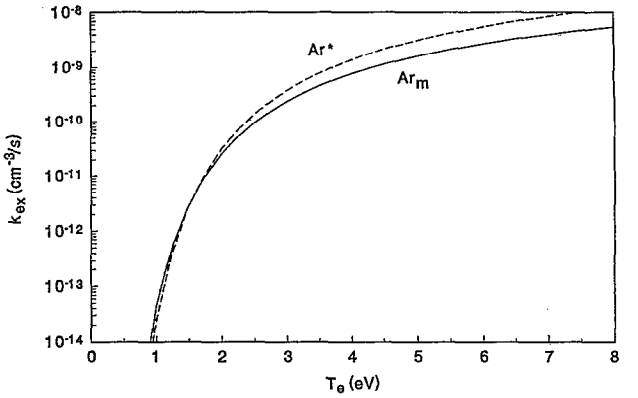

FIG. 8. Comparison of excitation rate constants as a function of electron temperature for the Ar metastable and excited states based on the Arrhenius expressions from Ref. 23.

where Ar is neutral argon, e is an electron, Ar_m is metastable argon, Ar* is excited-state argon, and Ar_r is the argon resonant $4s$ state, Ar^+ is the argon ion, and $h\nu$ is the energy of an emitted photon.

We can gain some insight into the changes in our measured metastable distributions by comparing them to the Ar $5p\rightarrow 4s$ optical emission distribution. This comparison is useful because the time-averaged optical emission (qualitatively) indicates the spatially dependent electron-impact excitation of the metastables, whereas the metastable distribution largely reflects the balance between the electron-impact production of metastables and the various destruction mechanisms noted above. (Note that here the spatial distribution of the emission is not affected by diffusion because of the relatively short radiative lifetime of the $5p$ state, and is not affected by two-body collisional de-excitation because the argon neutral, i.e., the dominant quencher, density is uniform.) Thus, by comparing the metastable and emission distributions, we can potentially see what effect the loss mechanisms have on the resulting spatial distribution of metastables.

Before making these comparisons we should emphasize that, strictly speaking, the $5p\rightarrow 4s$ emission is proportional to the total electron-impact excitation (including direct and cascade excitation) of the $5p$ state. However, because the excitation processes for the metastable and $5p$ states are similar, the $5p\rightarrow 4s$ emission should qualitatively indicate the excitation rate of the metastables, at least to the extent that the direct excitation processes dominate. This assertion can be justified to some extent by noting the similarity of the excitation rate coefficients for argon metastables and excited states shown in Fig. 8. The rate coefficients shown in this figure were calculated (using the rate expressions from Ref. 23) by assuming a Maxwellian distribution for electrons and modeling the excited states of argon with one metastable state (11.6 eV) and one radiative excited state (13.2 eV). While both of these assumptions are simplifications for the rf plasmas considered here, the excitation rate coefficients in Fig. 8 presumably show the correct qualitative trends.

For simplicity, we compare centerline axial profiles of the metastable density to line-of-sight-integrated profiles of the Ar $5p\rightarrow 4s$ plasma emission between 410–450 nm. Fig-

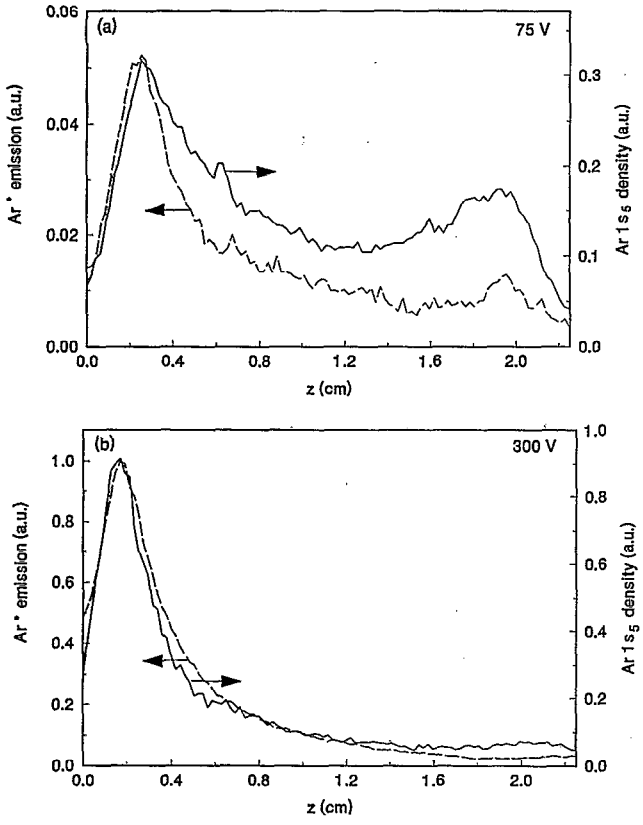

FIG. 9. Comparison of centerline Ar $1s_5$ metastable (LIF) and the line-of-sight-integrated $5p \rightarrow 4s$ excited-state emission profiles at 133.3 Pa (1000 mT) and an applied voltage of (a) 75 V and (b) 300 V.

ure 9 shows a typical comparison of optical emission and metastable density profiles for experiments at 133.3 Pa and 75 and 300 V, respectively. As illustrated in the figure, the metastable and emission profiles are qualitatively similar, although, in some cases (especially at lower voltages), the metastable profiles are somewhat broader than the emission profiles, presumably due to metastable diffusion. Similar trends were also observed for the lower pressure cases, although at 13.3 Pa the broadening of the metastable profiles was less dependent upon the applied voltage.

The similarities in the corresponding metastable and emission profiles indicate that, in these low-pressure argon discharges, the metastable distribution is largely determined by the spatially dependent electron-impact excitation function. Nevertheless, it is important to realize that differences in the relative rates of metastable loss mechanisms at various conditions can significantly affect the resulting metastable distributions. In Fig. 9(b), for example, the profiles are nearly identical, suggesting that diffusion is negligible and the other collisional loss rate balance the electron-impact production of metastables. In contrast, at lower voltages and/or pressures, diffusion is more significant relative to the collisional losses and, consequently, metastable profiles are broadened. For example, in Fig. 9(a) the metastables produced near the plasma/sheath interface diffuse into the plasma bulk prior to quenching and lead to an apparent buildup of metastables, when one compares the metastable and emission (i.e., metastable production) profiles.

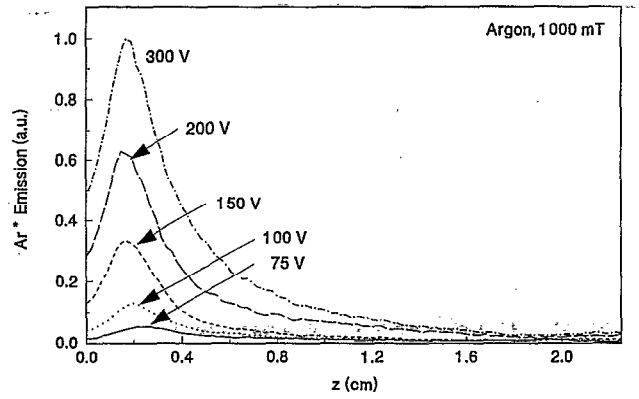

FIG. 10. Centerline line-of-sight-integrated argon excited-state emission profiles ($5p \rightarrow 4s$) at 133.3 Pa (1000 mT) and applied voltages of 75–300 V.

The significance of the combined loss mechanisms in determining the resulting metastable distribution is also illustrated by comparing the 133.3 Pa centerline excited-state emission profiles in Fig. 10 to the metastable profiles shown previously in Fig. 7(b). In particular, note that the emission profiles indicate that the metastable production near the powered sheath/bulk interface increases monotonically (and significantly) as the applied voltage is increased from 75 to 300 V, while the resulting peak metastable density shows a nonmonotonic behavior, as discussed above. Since the local metastable production continues to increase with applied voltage, the observed saturation and subsequent decrease in peak metastable density must result from a relatively larger increase in the total local metastable loss rate. From these measurements alone, however, we cannot determine which loss mechanism(s) are responsible. The increased quenching could result from an increase in the diffusional losses to the powered electrode, the electron quenching and excitation of metastables, and/or the metastable pooling reaction. Future modeling work is planned to examine these observed trends.

In Figs. 10 and 7(b), we also observe contrasting behaviors in the metastable production (indicated by emission) and the resulting metastable density at the center of the plasma ($z \sim 1$ cm). Once again the emission (Fig. 10) suggests a monotonic increase in production of metastables, but the observed metastable density [Fig. 7(b)] actually decreases monotonically. This observed decrease in metastable density in the bulk is presumably caused by an increase in electron quenching within the plasma bulk, which results from the increased electron number density at higher voltages. For these conditions, electron quenching to nearby resonant states is expected to dominate within the plasma bulk, because of the electron number density is largest near the center of the plasma and the electron energy is relatively low.[8]

SUMMARY AND CONCLUDING REMARKS

Two-dimensional, relative measurements of the argon $1s_5$ metastable density field within a low-pressure, glow discharge have been obtained using planar laser-induced fluorescence imaging. The measurements were conducted using a GEC rf reference cell and results were reported for pure argon discharges with pressures ranging from 13.3 to 133.3

Pa and applied peak-to-peak voltages of 75–300 V. While these results provide relative rather than absolute densities, they represent one of the first sets of detailed 2D measurements of the argon metastable distribution in an rf glow discharge, and should be useful for 2D plasma model validations.

The measured metastable distributions generally show significant radial and axial variations that depend more strongly on pressure than applied voltage. For all conditions examined, the metastable density increases radially from the center of the discharge to the edge of the plasma (from ~10% to ~30%), but is generally more radially uniform at higher voltages. As the pressure is increased from 13.3 to 133.3 Pa, the axial distribution changes from a center-peaked parabolic-like profile to an asymmetrical profile peaked near the powered electrode, and the peak density increases by a factor of ~4. Comparisons of the centerline-axial metastable and optical emission profiles indicate that, while the metastable distribution is largely determined by the spatially dependent electron-impact excitation function, differences in the relative rates of metastable loss mechanisms at various conditions can significantly affect the resulting metastable distributions.

ACKNOWLEDGMENTS

The authors would like to thank M. A. Sobolewski and J. R. Whetstone for their help with the plasma electrical measurements, and J. K. Olthoff, M. J. Kushner, and D. J. Economou for helpful discussions regarding this work.

[1] *Plasma Etching: An Introduction,* edited by D. M. Manos and D. L. Flamm (Academic, Boston, 1989).
[2] D. P. Lymberopoulos and D. J. Economou, Appl. Phys. Lett. **63**, 2478 (1993); see also, J. Vac. Sci. Technol. A **12**, 1229 (1994).
[3] D. P. Lymberopoulos and D. J. Economou, J. Appl. Phys. **73**, 3668 (1993).
[4] M. Meyyappan, in *Computational Modeling in Semiconductor Processing,* edited by M. Meyyappan (Artech House, Boston, 1995), and references therein.
[5] A collection of papers on the modeling of collisional low-temperature plasmas can be found in a special issue section of IEEE Trans. Plasma Sci. **19** (1991).
[6] B. L. Preppernau and T. A. Miller, in *Glow Discharge Spectroscopies,* edited by R. K. Marcus (Plenum, New York, 1993).
[7] K. E. Greenberg and G. A. Hebner, J. Appl. Phys. **73**, 8126 (1993).
[8] R. A. Gottscho, G. R. Scheller, T. Intrator, and D. B. Graves, J. Vac. Sci. Technol. A **6**, 1393 (1988).
[9] G. R. Scheller, R. A. Gottscho, T. Intrator, and D. B. Graves, J. Appl. Phys. **64**, 4384 (1988).
[10] G. R. Scheller, R. A. Gottscho, D. B. Graves, and T. Intrator, J. Appl. Phys. **64**, 598 (1988).
[11] L. Sansonnens, A. A. Howling, Ch. Hollenstein, J.-L. Dorier, and U. Kroll, J. Phys. D **27**, 1406 (1994).
[12] F. Tochikubo, Z. L. Petrović, S. Kakuta, N. Nakano, and T. Makabe, Jpn. J. Appl. Phys. **33**, 4271 (1994).
[13] P. J. Hargis, Jr., K. E. Greenberg, P. A. Miller, J. B. Gerardo, J. R. Torczynski, M. E. Riley, G. A. Hebner, J. R. Roberts, J. K. Olthoff, J. R. Whetstone, R. J. Van Brunt, M. A. Sobolewski, H. M. Anderson, M. P. Splichal, J. L. Mock, P. Bletzinger, A. Garscadden, R. A. Gottscho, G. Selwyn, M. Dalvie, J. E. Heidenreich, J. W. Butterbaugh, M. L. Brake, M. L. Passow, J. Pender, A. Lujan, M. E. Elta, D. B. Graves, H. H. Sawin, M. J. Kushner, J. T. Verdeyen, R. Horwath, and T. R. Turner, Rev. Sci. Instrum. **65**, 140 (1994).
[14] D. H. Stedman and D. W. Setser, in *Progress in Reaction Kinetics*, edited by K. R. Jennings and R. B. Cundall (Pergamon, New York, 1971), Vol. 6, Part 4.
[15] R. K. Hanson, J. M. Seitzman, and P. H. Paul, Appl. Phys. B **50**, 441 (1990).
[16] M. A. Sobolewski, J. Vac. Sci. Technol. A **10**, 3550 (1992).
[17] W. L. Wiese, J. W. Brault, K. Danzmann, V. Helbig, and M. Kock, Phys. Rev. A **39**, 2461 (1989).
[18] The electron quench rate of the $5p$ $(3p_2)$ state was estimated from the value of argon metastable-to-resonant level quenching by electrons reported by C. M. Ferreira, J. Loureiro, and A. Ricard, J. Appl. Phys. **57**, 82 (1985).
[19] G. Inoue, D. W. Setser, and N. Sadeghi, J. Chem. Phys. **76**, 977 (1982).
[20] L. J. Overzet and M. B. Hopkins, Appl. Phys. Lett. **63**, 2484 (1993).
[21] C. M. Ferreira and J. Loureiro, J. Phys. D **16**, 1611 (1983).
[22] N. L. Bassett and D. J. Economou, J. Appl. Phys. **75**, 1931 (1994).
[23] F. Kannari, M. Obara, and T. Fujioka, J. Appl. Phys. **57**, 4309 (1985).